GN&C Subsystem Concept for Safe Precision Landing of the Proposed Lunar MARE Robotic Science Mission

John M. Carson III[1,4,*], Andrew E. Johnson[4,†], F. Scott Anderson[2,‡], Gerald L. Condon[1,§], Louis H. Nguyen[1,◇], Jon B. Olansen[1,▽], Jennifer L. Devolites[1,¶], William J. Harris[1,★], Glenn D. Hines[5,‖], David E. Lee[1,**], Farzin Amzajerdian[5,††], Nikolas Trawny[4,‡‡], Samuel Lawrence[3,§§], Andres Huertas[4,◇◇], Wyatt Johnson[1,▽▽]

[1]*NASA Johnson Space Center,* [2]*Southwest Research Institute,* [3]*Arizona State University*
[4]*Jet Propulsion Laboratory, California Institute of Technology,* [5]*NASA Langley Research Center*

The MARE (Moon Age and Regolith Explorer) Discovery Mission concept targets delivery of a science payload to within a 100-meter radius of a specified landing site on the lunar surface for sample collection and dating. The mission science is within a region of smooth lunar maria terrain near Aristarchus crater that includes surface features, such as small sharp craters and rocks, that present landing hazards to the spacecraft. For successful delivery of the science payload to the surface, the vehicle Guidance, Navigation and Control (GN&C) subsystem requires safe and precise soft landing capability, so the design infuses the NASA Autonomous precision Landing and Hazard Avoidance Technology (ALHAT) and a gimbaled, throttleable LOX/LCH$_4$ main engine. The ALHAT system implemented for MARE is a specialization of prototype technologies in work within NASA, including a passive optical Terrain Relative Navigation (TRN) sensor, a Navigation Doppler Lidar (NDL) velocity and range sensor, and a Lidar-based Hazard Detection (HD) sensor. The landing descent profile is from a retrograde orbit over lighted terrain with landing near lunar dawn. The GN&C subsystem with ALHAT capabilities will deliver the science payload to the lunar surface within a 20-meter radius of the targeted landing location and at a site having greater than 99% safety probability, which minimizes risk to safe landing and delivery of the MARE science payload to the intended terrain region.

I. Introduction

A GN&C subsystem design concept has been developed to safely and precisely deliver the science payload for the proposed MARE Discovery Mission to the surface of the Moon. The mission science targets a smooth, basaltic lunar mare terrain region near Aristarchus crater that contains hundreds of candidate landing sites that can satisfy the science objectives. Detailed analysis of the most desirable science locations led to the development of a mission functional requirement on the spacecraft GN&C subsystem to deliver the science

*GN&C Lead, JSC-IPA, Ph.D., AIAA Associate Fellow.
†TRN/HD Lead Analyst, Ph.D., AIAA Senior Member.
‡Mission Principal Investigator, Ph.D.
§Mission Design and Analysis.
◇Control Analysis, AIAA Senior Member.
▽Deputy Project Manager, Ph.D., AIAA Senior Member.
¶Deputy Project Systems Engineer.
★Mission Proposal Manager.
‖NDL Chief Engineer.
**Mission and Trajectory Design.
††NDL Chief Scientist, Ph.D., AIAA Member.
‡‡TRN/HD Lead Engineer, Ph.D., AIAA Member.
§§Mission Science Team, Ph.D.
◇◇Terrain Maps and Hazards Analysis, Ph.D., *retired.*
▽▽Navigation Analysis, Ph.D., now at *Intuitive Machines.*

payload to within a 100-meter radius landing ellipse of the selected site. The terrain characteristics in the desirable landing regions include features such as small, sharp craters and small boulders that pose quantifiable risk to safe landing, and therefore a risk to successful surface science operations. The safe and precise soft landing of the NASA Autonomous Vehicle for In-situ Science (NAVIS), developed by JSC for the MARE mission, is accomplished through infusion of NASA Autonomous precision Landing and Hazard Avoidance Technology (ALHAT)[1,2] into the GN&C subsystem and infusion of a gimbaled, throttleable LOX/LCH_4 main engine. The GN&C design enables precise descent Navigation of the NAVIS spacecraft and onboard detection of landing sites safe from lander-sized hazards (to greater than 99% safety probability). The NAVIS GN&C design ensures a safe and precise soft landing within a 20-meter radius ellipse of the target science site, which minimizes risk to safe landing and provides significant margin to ensure landing within the target ellipse.

The science objectives of the MARE mission are to revolutionize understanding of (1) the impact history of the inner solar system, and (2) the evolution and differentiation of the interiors of one-plate planets. The mission will accomplish these goals by landing on a young, nearside lunar lava flow and collecting and analyzing samples to measure their radiometric ages, geochemistry, and mineralogy. These measured ages, when related to the number of craters at the site, will redefine the crater-based chronology models that form the basis of much of our understanding of inner solar-system history. The compositional data on the young lava will reveal how the Moon's interior and, by extension, those of the other terrestrial planets have evolved through time. The MARE mission proposal is a partnership between the Southwest Research Institute (SwRI), the NASA Johnson Space Center (JSC), and multiple supporting organizations, which include the NASA ALHAT team and Arizona State University (ASU).

The development of ALHAT capabilities has been driven by long term NASA interests to develop safe and precise landing capabilities that enable mission science at terrain locations that pose a significant risk to safe landing or to rover traverses, as well as to enable safe touchdown in the proximity of pre-existing surface assets (e.g., sample caches, assent vehicles, crew assets, etc.). The National Research Council (NRC) has likewise identified safe and precise landing technologies as a high priority need for future Entry, Descent and Landing (EDL) missions for similar reasons.[3] The development of ALHAT has been a cross-NASA effort over the past two decades and includes engineers and scientists from JSC, Jet Propulsion Laboratory (JPL), and Langley Research Center (LaRC).

This paper provides an overview of the MARE concept science mission, with a focus on the GN&C subsystem for precisely delivering the mission science payload. An overview of the mission science is provided in Section II, and an overview of the NAVIS spacecraft and the GN&C subsystem are provided in Section III. The mission design and descent operations concept are discussed in Section IV, and Section V provides some select GN&C analyses used to inform the NAVIS concept design for the MARE proposal. Summary remarks are provided in Section VI.

II. Mission Science Overview

Recent crater count analyses have emphasized that we are confident in only 25% of solar system history.[4] Current models of inner solar system chronology have billion-year uncertainties during the period from one- to three-billion years ago, due to a lack of lunar samples with well understood provenance. This uncertainty fundamentally affects our understanding of events in solar system history, such as the duration and evolution of volcanism on the Moon, duration of the era of water and volcanism for Mars, and the bombardment environment under which life evolved on Earth (Figure 1). To close this critical gap in lunar chronology, the MARE Discovery-class mission was proposed. Only by returning to the Moon to fill these sampling gaps can the cratering models be corrected, delivering results of far-reaching importance that span multiple planetary bodies. The MARE mission directly addresses high-priority Decadal Survey goals for new lunar age determinations: "Priority mission goals include... the reconstruction of the impact history of the inner solar system through the exploration of better characterized and newly revealed lunar terrains".[5]

Understanding the relative timing of geologic events by using crater counting is the keystone to unraveling the history recorded on the surfaces of rocky bodies. Crater counts, in conjunction with radiometrically-

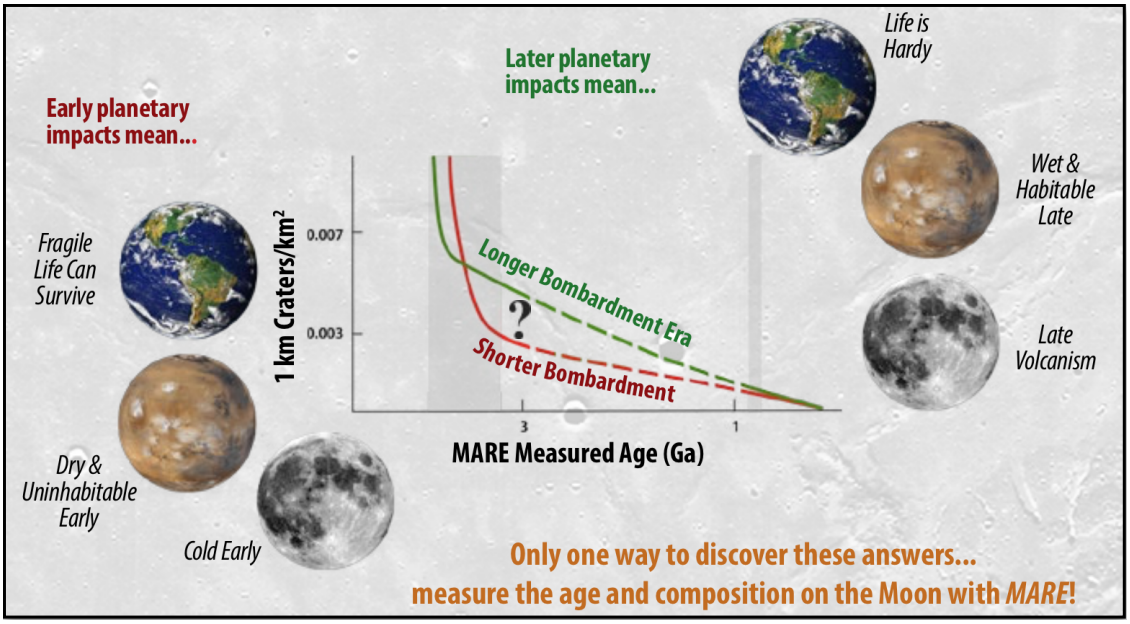

Figure 1. Which Solar-System history is true?

dated Apollo and Luna samples, have been used to estimate the absolute ages of events on the Moon.[6] The resulting cratering flux has been extrapolated to Mars,[7] Mercury,[8,9] Venus,[10] Vesta,[11–13] and used in models of early solar system dynamics.[14] However, recent analysis[4] indicates four major complications to the crater chronology picture: a) crater-counted terrains may not be the sources of dated samples, b) the need to extrapolate crater count relationships to very young and old terrains, c) crater counts of the sampled terrains result in a wide range of N(1) crater densities, used to model the age of a surface, and d) new data from the LRO (Lunar Reconnaissance Orbiter) Camera (LROC) is revealing many more craters than previously observed.

These problems result in billion-year uncertainties for the history of the Moon[4] and solar system. For example, the era of bombardment of the inner solar system, as recorded by lunar impacts, may have effectively ended ∼3.7 Ga ago, or at some younger time. Because life on Earth is thought to have arisen between ∼3.7 and ∼3.0 Ga ago, the model improvement could reveal new insights about the habitability of the early Earth. Similarly, the era of liquid water on the Martian surface, which is intimately related to possible life on Mars, as well as the eras of voluminous volcanism on the Moon and Mars, might have ended ∼3 Ga ago, or extended to as recently as ∼1.7 Ga ago. The key to addressing these issues is dating additional samples with well understood provenance, from terrain with undisputed crater counts, and from terrains of age 1-3 Ga. The young lava flows southwest of Aristarchus are ideally suited for this purpose.

After landing southwest of the Aristarchus plateau, samples within reach of the NAVIS lander arm will be assessed, by using onboard imaging and near/thermal infrared mineralogy instruments, and then ranked and prioritized for analysis. The analysis process consists of retrieving a sample with the arm, preparing the sample surface with a grinder, and interrogating that surface for chronologic and compositional information with the Chemistry and Dating EXperiment (CDEX). Visible and infrared landing-site context measurements will be interfingered with geochronology and chemistry analyses throughout the day. A second full lunar day of science measurements is planned as operational margin to ensure mission success.

MARE microscopic geochemistry, mineralogy, and imaging will be used to determine the petrology, and hence the thermal and magmatic history, of young mare flows and then place them in local and regional context. These MARE measurements will provide the first ground-truth for correlation with lunar orbital data, including directly comparable thermophysical and mineralogical measurements. Only MARE can perform this combination of measurements on the Moon, supplying the data required to write fundamentally new chapters of inner solar system history.

III. Spacecraft and GN&C Subsystem Overview

The NAVIS spacecraft design is optimized to support mission science. The top deck of the spacecraft supports the power, avionics, communication, some of the GN&C electronics and hardware, and the static science equipment (not arm mounted), which enables efficient, centralized thermal control for all components. The equipment on the top deck plates is almost completely shrouded by solar panels and radiators, leaving an opening for robotic arm access; the arm is mounted to a landing leg for surface access. Other GN&C and communication instruments, such as antennae, are attached to other landing legs to provide unobstructed fields of view. Figure 2 illustrates the NAVIS spacecraft and includes pointers to visible GN&C, propulsion and robotic arm components. The NAVIS design benefits from the extensive technology maturation of the ALHAT precision landing system and the LOX/LCH_4 propulsion system, advanced through 63 integrated flight tests of the NASA Morpheus vehicle and through continued development efforts through other NASA technology development programs.[15−26]

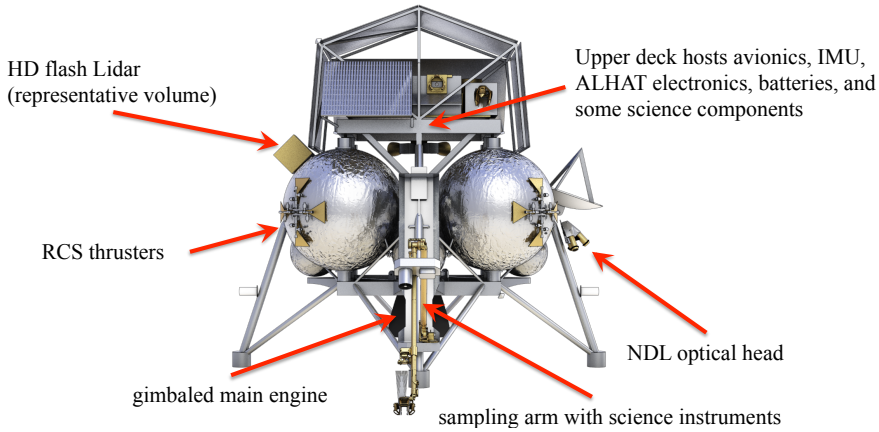

Figure 2. The MARE NAVIS spacecraft with some visible GN&C, Science, and Propulsion components indicated. Note that the sun sensors, TRN camera, and star trackers are not visible.

The NAVIS GN&C and Propulsion subsystems enable delivery of the MARE science payload to within a 20 m radius landing ellipse at the designated mission science site. Inclusion of NASA ALHAT capabilities onboard the NAVIS provides the situational awareness necessary for the GN&C subsystem to command vehicle maneuvers for a safe and precise soft landing. The throttleable and gimbaled LOX/LCH_4 main engine and 16 Reaction Control System (RCS) thrusters within the Propulsion subsystem likewise provide the precise execution and control authority necessary to implement the GN&C commands for the precise landing at the identified safe location.

The GN&C subsystem design provides onboard functionality during lunar transfer and orbital operations, as well as during powered descent to landing. During lunar transfer and orbital operations, the GN&C subsystem conducts autonomous Attitude Determination and Control (ADC) with the onboard Kalman filter processing vehicle Inertial Measurement Unit (IMU) and star tracker data to estimate attitude and rotational rates and the onboard attitude-control logic providing commands to the RCS engines. Trajectory Correction Maneuvers (TCMs) are planned and sequenced from the ground utilizing ground based Deep Space Network (DSN) navigation data and mission planning tools, and the TCM burns are executed onboard with a coordinated pointing maneuver and the Thrust Vector Control (TVC) capability of the main engine. During the powered descent to landing, the GN&C subsystem is fully autonomous, with full state (attitude and translation) navigation, attitude control, and translational guidance. No ground intervention is used (or feasible) during powered descent and landing. Coordinated attitude and translational control during powered descent uses steering logic to convert the guidance profile into TVC of the main engine (for vehicle translation and control of two rotational DOFs – pitch and yaw) and roll control with the RCS.

The GN&C sensor suite includes several high-TRL (Technology Readiness Level) sensors, along with the prototype NASA-developed ALHAT system. The non-ALHAT sensors include one Honeywell Miniature

Inertial Measurement Unit (MIMU), two Sodern Star Trackers, and four Adcole Pyramid Coarse Sun Sensors (CSSs). The Honeywell MIMU includes gyroscopes and accelerometers to measure 3-axis rotation rates and 3-axis translational acceleration. The MIMU is TRL 9 and has successfully launched on over 40 space missions. The Sodern Hydra Star Trackers include one Electronics Unit (EU) and two Optic Heads (OH). The Hydra is TRL 9 and multiple units are in current operation in space onboard the SPOT-6 spacecraft launched in 2012, and the SPOT-7, KazEOSat-1 and KazEAOSat-2 spacecrafts that all launched in 2014. The Adcole Pyramid CSSs have a 2-pi steradian viewing cone and are electrically-passive sensors, making them ideal for use onboard the NAVIS for recovery and safe mode operations. The Pyramid CSS is TRL 9 and has more than 20 years of cumulative spaceflight heritage.

The ALHAT components include sensors, avionics, and algorithms at various TRLs. Figure 3 provides images of the sensor hardware used for the various ALHAT components, which include a Navigation Doppler Lidar (NDL), a Terrain Relative Navigation (TRN) system, and a Hazard Detection (HD) system. The NDL (Figure 3, left) for MARE will be developed and delivered by NASA LaRC. The NDL incorporates a three-beam optical head and a custom electronics unit that houses a laser and multiple electronics subassemblies. The TRN system and HD system for MARE will be developed and delivered by NASA JPL; processing will be performed on a dedicated processor card within the primary spacecraft avionics unit. The TRN system incorporates a Malin Space Science Systems (MSSS) ECAM M50 camera (Figure 3, top right), and the HD system incorporates an Advanced Scientific Concepts (ASC) GEO3D GoldenEye flash Lidar (Figure 3, bottom right).

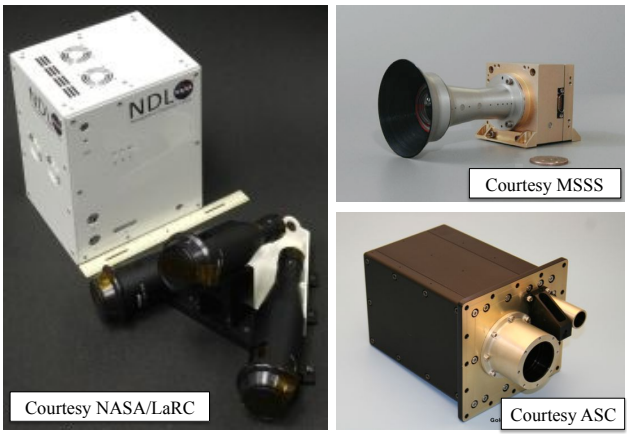

Figure 3. Images of ALHAT components: terrestrial-test prototype NDL (left) with 12-inch ruler for scale; TRN camera – MSSS ECAM M50 (right, top) with coin for scale; HD flash Lidar – ASC GEO3D GoldenEye (right, bottom)

The ALHAT NDL uses optical homodyne detection of a frequency-modulated, continuous waveform laser beam split into three separate output beams to produce highly accurate measurements of Line-of-Sight (LOS) velocity and range.[27,28] The beams have angular separation that enable determination of velocity to within 2.5 cm/s and altitude to within 1 m when combining the three LOS beam measurements, each with a range and speed, within the onboard Navigation filter. The prototype NDL can measure LOS velocities up to 200 m/s and LOS ranges up to 4 km. The previous-generation prototype NDL is currently at TRL 5 and has been extensively tested by LaRC onboard a helicopter and the Morpheus Vertical Testbed (VTB) in lunar-like descent profiles. Future testing of the upgraded prototype NDL in Figure 3 (left), which achieves the desired MARE descent performance, is planned onboard a commercial rocket-propelled VTB as part of the ALHAT CoOperative Blending of Autonomous Landing Technologies (COBALT) flight demonstration funded by the NASA Advanced Exploration Systems (AES) Program and the NASA Flight Opportunities (FO) Program. The NDL electronics subassemblies make use of several existing TRL 9 components, as well as components that are being matured through ongoing development efforts within NASA in preparation for flight infusion. The NDL has a development path that will achieve TRL 6 prior to mission Preliminary Design Review (PDR).

The ALHAT TRN system provides global position knowledge that GN&C uses to plan descent maneuvers that minimize the landing position dispersions about the targeted science site. The TRN system uses a passive optical camera, a monochrome ECAM M50, for capturing real-time terrain images for onboard comparison with *a-priori* reconnaissance imagery and Digital Elevation Models (DEMs) stored in onboard memory. The reconnaissance data comes from existing Lunar Mapping and Modeling Project (LMMP) data, JAXA data, and new imagery from recent LRO orbital passes near the MARE science region. The TRN software executes on a dedicated RAD750 within the MARE avionics unit with TRN measurement updates every 20 seconds. The ECAM M50 has a 77-degree by 55-degree Field of View (FOV), which provides a large margin for terrain imaging during lunar descent to construct TRN measurements. The ECAM M50 will be TRL 8 upon delivery to the NASA Science Mission Directorate (SMD) OSIRIS-REx mission in June 2015 and TRL 9 following launch in September 2016. The TRN algorithms were developed by JPL and tested to TRL 6 onboard a helicopter and a NASA FO Program rocket-propelled VTB in 2014.

The ALHAT HD system uses a 128x128 pixel flash Lidar, an ASC GEO3D GoldenEye, with a 6° x 6° FOV to collect a three-dimensional (3D) point cloud of terrain data in real time and relative to the spacecraft. The data is analyzed onboard within 5 seconds to identify safe landing sites based NAVIS vehicle geometry and hazard tolerances (40 cm roughness and 10° slopes for the MARE NAVIS design). The analysis is performed with a HD algorithm that executes on the ALHAT-dedicated RAD750 within the MARE avionics. The HD capability generates a local measurement of terrain hazards that are undetectable in *a-priori* reconnaissance data, which minimizes landing risk for vehicles that have hazard tolerances smaller than the hazards detectable in reconnaissance data. The ASC GEO3D GoldenEye will be TRL 8 upon delivery to the NASA SMD OSIRIS-REx mission in June 2015, and TRL 9 following launch in September 2016. The HD algorithms and system has been in development, testing, and evolution within ALHAT and related projects for several years within NASA and have undergone numerous flight tests onboard helicopters and the Morpheus VTB.[16,29,30]

The NAVIS propulsion subsystem utilizes a GHe pressure-fed cryogenic LOX/LCH_4 propulsion system in which 2 oxygen propellant and 2 methane tanks fed propellants to the RCS engines and main engine through an integrated cryogenic feedsystem. The high performance and "green" LOX/LCH_4 is clean-burning, non-toxic, and space-storable. The Morpheus VTB successfully demonstrated this single-stage LOX/LCH_4 technology capability at a vehicle system level.[22] The propellant tanks contained slosh baffles,[23] and the feedsystem was designed to maintain equal propellant draining for the four propellant tanks.[24] These design elements are retained in the NAVIS propulsion system design. For the MARE mission, the NAVIS vehicle uses the single-stage propulsion system to perform all vehicle maneuvers (for a total mission ΔV of 2987 m/s) that occur following launch vehicle separation, which is after the launch-vehicle performs a Trans-Lunar Injection (TLI) burn. The main engine[25] is continuously throttleable at a 5:1 ratio, with thrust from 7900 N to 1580 N. The RCS is comprised of sixteen 31-N LOX/LCH4 engines, which ensures redundancy for enhanced mission reliability. Pulsing the RCS engines on for 40 ms with fast-response cryogenic solenoid valves provides a Minimum Impulse Bit (MIB) of 0.35 N-s to ensure vehicle control stability. MIB durations of 40 ms were demonstrated on the Morpheus VTB in 2014 for a scaled 80-N version of the RCS engines.[26] The MIB produces a rate increment (i.e. angular rate change for MIB firing) at 1/4 of the control rate deadband (i.e. upper to lower rate limit), providing 300% margin against limit cycling.

IV. Mission Design and Precision Landing Operations Concept

The trajectory design for the MARE mission provides adequate performance to set a spacecraft down at the specified lunar latitude and longitude for the mission science (latitude = 23.4°, longitude = -60°, altitude = 0 m) and at a desired epoch, while meeting associated vehicle and trajectory requirements. Launch readiness is targeted for 2021. The mission design produces monthly mission opportunities with multiple daily launch opportunities for each monthly opportunity. Figure 4 illustrates the mission events.

The MARE mission launches (Figure 4, Event 1) due east on an Atlas V 411. The launch vehicle delivers the MARE NAVIS spacecraft to a temporary Low Earth Orbit (LEO) (Event 2) that is nearly coplanar with the lunar transfer orbit. After LEO insertion, the combined upper stage and MARE NAVIS

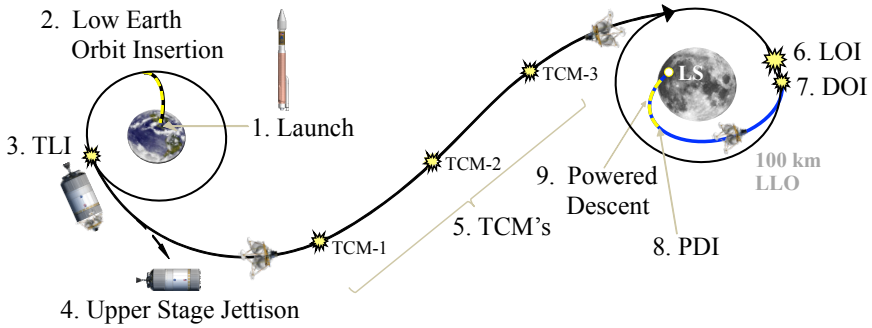

Figure 4. Illustration of MARE Mission Trajectory Events

spacecraft coasts to a preferred phase location for the TLI burn (Event 3), which achieves a transfer target to a lunar intercept anywhere from 3 to 8 days after Earth departure, depending upon the selection of one of several daily launch opportunities in a particular month. After TLI, the MARE NAVIS spacecraft separates from the booster upper stage (Event 4), and the upper stage performs a retargeting maneuver for a safe disposal. The spacecraft continues on a trans-lunar coast to a Lunar Orbit Insertion (LOI) target and performs all post-TLI propulsive maneuvers with the onboard propulsion system. While en-route to LOI, the outbound trajectory design accommodates three (and optionally four) Trajectory Correction Maneuvers (TCMs). These TCMs (Events 5) are only performed if the spacecraft trajectory is significantly dispersed from its planned trajectory.

At lunar arrival, the LOI maneuver (Event 6) places the MARE NAVIS spacecraft into a retrograde 100 km-altitude circular Low Lunar Orbit (LLO). The retrograde LLO (in conjunction with the launch epoch) ensures that the landing phase will occur over sunlit terrain, with the sun behind the spacecraft at a low elevation angle of approximately 10°. This sun angle provides adequate lighting for successful ALHAT TRN and lands the MARE NAVIS spacecraft near lunar dawn. The spacecraft remains in LLO for approximately 3-4 revolutions during which time the ground-based orbit determination/navigation prepares for the Descent Orbit Initiation (DOI) maneuver (Event 7). The DOI maneuver reduces the pericynthion from 100 km to about 15 km altitude. Variation in the post-DOI periapsis altitude does not have a strong impact on the powered descent ΔV cost, so a positive pericynthion provides a once around capability in the event of a failed Powered Descent Initiation (PDI) maneuver (Event 8), thus enhancing the possibility of mission success with negligible performance impact. PDI marks the beginning of the powered descent arc (Event 9): a continuous main engine burn which ends with touchdown on the surface of the Moon. PDI occurs near pericynthion, about a half a rev after the DOI maneuver (about an hour).

Figure 5 illustrates the nominal powered descent profile to the lunar surface and includes the onboard Guidance segments and the active periods for GN&C sensors, including ALHAT sensors. The powered descent consists of the following segments: Braking, Pitch Up/Throttle Down, Approach, Divert, Pitch to Vertical, and Terminal Vertical Descent (TVD) to touchdown. The ALHAT sensors include passive-optical Terrain Relative Navigation (TRN), Navigation Doppler Lidar (NDL) velocimetry/ranging, and HD (Hazard Detection) for safe landing site determination. A specialized descent Navigation filter fuses the ALHAT measurements to provide global and local state knowledge to ensure precise and safe soft landing within the targeted science region. An onboard Autonomous Flight Manager (AFM) monitors both the descent timeline and navigation states to trigger each guidance mode, sequence the ALHAT sensors and control spacecraft attitude.

The PDI burn initiates the Braking phase, a fuel-optimal maneuver, which uses a high throttle setting to efficiently reduce energy. The onboard Navigation filter used during powered descent is initialized from the ground tracking state following the final Deep Space Network (DSN) observation of the MARE NAVIS vehicle that occurs approximately 90 minutes prior to the DOI burn. Following this initialization, the Navigation estimate is updated with onboard measurements from the vehicle IMU (and initially two star trackers prior to the PDI burn) until the TRN system is active at approximately 13 km altitude down to approximately

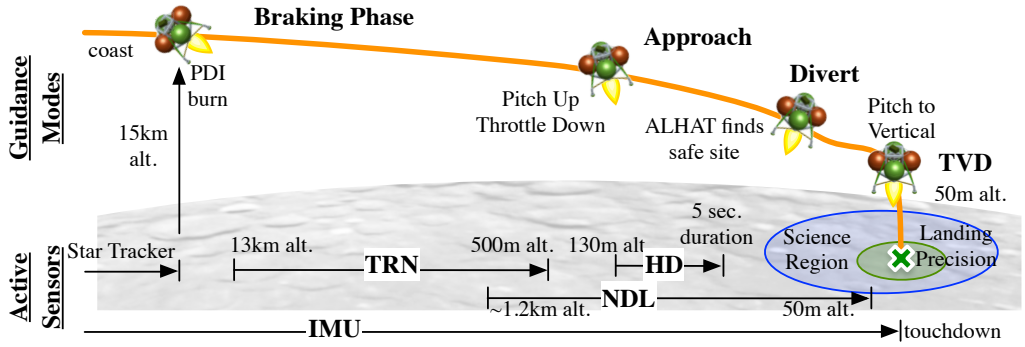

Figure 5. Nominal Powered Descent Profile with Guidance Modes and Active ALHAT Sensors

500 meters altitude.

The NDL is active from approximately 1.2 km altitude until approximately 50 meters altitude. The NDL measurements commence prior to the completion of TRN, which ensures a blended steady-state Navigation filter solution and minimization of filter position error growth following TRN cutoff. The NDL optical head (illustrated on the spacecraft in Figure 2) is positioned so that the three beams nominally point in the forward direction of flight during Braking and toward the aft direction of flight during Approach. The Approach phase pitches the vehicle up to 80° at reduced throttle and sets up for onboard Hazard Detection (HD) at a 130 meter altitude (and a 160 meter slant range to the initial landing target). Analysis of smooth lunar maria terrain with up to 10% rock abundance, the terrain type for the MARE science, indicates abundant safe sites reachable within a 10-meter divert, which together with the GN&C knowledge uncertainty provides safe pinpoint landing to greater than 99% probability within the 20 m radius (3-sigma) landing ellipse.

The safest landing site identified through HD is passed to the onboard AFM, which initiates a Guidance re-plan and commands a small, subsequent Divert maneuver to start TVD from above the safe landing site. The onboard Navigation filter continues to process high-precision NDL velocity measurements and LOS range measurements through Approach and Divert, which enables onboard GN&C to autonomously command maneuvers to minimize lateral vehicle velocities to establish TVD from 50 meters altitude above the safe site. The NDL is shut off below approximate 30 meters altitude during TVD to avoid spurious measurements that could occur when dust is kicked up from the plume-soil interaction. The Navigation filter dead reckons on the IMU during this final segment, which ends with a 1 m/s downward velocity touchdown on the lunar surface. During TVD, the NAVIS spacecraft is also oriented to point the radiators toward local North and the solar array centerline to within 5° of the local East-West line, maximizing thermal dissipation and power generation. Touchdown is sensed with onboard contact logic that is based on algorithms developed and repeatedly tested on Morpheus. The combination of the direct NDL velocity measurements following TRN and the final dead reckoning on the high-precision IMU minimizes Navigation error growth in position and velocity estimates and ensures a soft touchdown. Touchdown occurs shortly after lunar dawn (with a Sun elevation of 10°), which maximizes the amount of sunlight time for surface science operations. Touchdown on the surface begins the surface operations phase.

V. GN&C Performance Analysis

V.A. Landing-Ellipse Analysis

A LinCov (Linear Covariance) analysis was performed on the descent Navigation system design. The analysis was used to assess GN&C ability to achieve a precise landing within the science target ellipse of 100-meter radius, including a hazard avoidance divert (of up to 10 meters) to the detected safe landing site. The LinCov analysis also facilitated a trade study of landing precision with different combinations of GN&C and ALHAT sensors. Note, that although the science requirement on GN&C was to land within a 100-meter

radius ellipse, the science goal was to land within a much tighter, 20-meter radius ellipse.

The LinCov analysis timeline started with the final ground-based Navigation update (prior to the DOI burn in lunar orbit) and ended with touchdown, which coincides with the timeline for NAVIS autonomous onboard Navigation. The analysis initialization was based on a nominal ground-based Navigation uncertainty for the final DSN observation of the NAVIS spacecraft in LLO. The descent trajectory timeline for active GN&C and ALHAT measurements followed the sensor sequence illustrated in Figure 5. Noise and bias models for the star tracker and MIMU were from published vendor specifications, and models of the ALHAT sensor uncertainties (TRN and NDL) were based on results from simulations and tests conducted within the ALHAT team. The positions and orientations for the optical sensors mimicked the layout onboard the NAVIS vehicle (Figure 2), and the trajectory profile came from the mission design trajectory.

Table 1 summarizes two LinCov analysis cases: one including both ALHAT TRN and ALHAT NDL (NDL provides both velocity and range), and one with ALHAT TRN and a spaceflight-qualified altimeter. The table entries summarize the 3-σ landing footprint uncertainty and the landing velocity uncertainty. The MIMU is used for both cases (the final attitude knowledge on landing is within $\pm 0.02^\circ$/axis, 3-σ).

Table 1. Two LinCov cases assessing different descent sensor combinations. Values are 3-σ.

Descent Sensors	Lateral Error (m)	Altitude Error (m)	Velocity Error (m/s)
TRN + NDL	6	0.8	0.03
TRN + Altimeter	19	0.7	0.2

Both options in the table clearly achieve the 100-meter radius requirement, with significant margin and including up to a 10-meter hazard avoidance divert. However, only the TRN + NDL option achieves the 20-meter radius science goal (when including the 10-meter hazard avoidance divert). This result supported inclusion of the NDL within the baseline NAVIS design, although the NDL was considered a potential descope option in the event of subsequent mission schedule or budget issues. Separately, the NASA Discovery Mission proposal solicitation encouraged infusion of ALHAT capabilities within missions, which also supported inclusion of the NDL within the baseline design.

The tight performance of the TRN+NDL option is enabled by the precise and direct velocity measurements from the NDL, along with its range measurements, that minimize Navigation position-error growth after the completion of TRN measurements. The combined TRN+NDL provided a final altitude uncertainty on par with the TRN+Altimeter option, as well. The TVD phase ends at a constant 1 m/s downward velocity with main engine shutdown planned between 2-3 meters altitude, which is within the altitude uncertainty, to reduce plume impingement on the local terrain and scattering of desired science samples. A preliminary assessment of this descent strategy shows that engine cutoff at 3 m altitude is also well within the design margin for the landing energy attenuation system.

V.B. Flight Control Analysis

The NAVIS spacecraft flight control analyses address all phases of NAVIS propulsive flight (Figure 4), which include lunar transit, LLO operations, and powered descent. For operations during lunar transit and in LLO, the Flight Control System (FCS) provides 3-axis rotational control for slewing and pointing the spacecraft for communication and for power and thermal balance. The FCS is also required to slew and maintain attitude control while performing delta-V burns with the main engine: TCMs, LOI and DOI. During the powered descent phase, the FCS provides 3-axis rotational control and executes the closed-loop guidance to maneuver and gently land the spacecraft at the ALHAT-detected safe landing site.

The LOX/LCH_4 RCS is sized to provide 3-axis rotational control with torque couples, which minimize translational disturbances. Control analyses investigated different RCS thrust magnitudes and profiles and their resultant angular rate increments to determine the required NAVIS thrust performance and MIB. The FCS design utilizes a phase plane logic for each rotation axis that is similar to that used on the Morpheus test vehicle.[31] Phase plane control parameters, attitude dead-bands, and attitude rate dead-bands are

determined based on the RCS thruster performance and MIB to target better than the ±5°/axis pointing accuracy required for solar array pointing. Long duration attitude hold simulation analyses in cis-lunar and LLO, using ±1°/axis and ±0.25°/sec/axis attitude and attitude rate dead-bands, demonstrated better than required attitude control performance and provided good estimates of RCS thruster firing duty cycle and propellant usage. Large angle rotational maneuvers (slews) utilize an Eigen-axis maneuver rate logic with selectable maneuver rate limit (0.15-1.0°/sec) to meet vehicle constraints and mission requirements. Cumulative thruster firing duty cycles from simulated operations throughout all phases of flight are utilized as design and qualification requirements for the RCS.

Translational control for powered descent uses a thrust vector control logic similar to that of the Morpheus vehicle.[31] An outer translational control loop is housed in the guidance function where a Proportional-Derivative (PD) feedback control law is applied to the vehicle position and velocity errors, with respect to the guidance trajectory, to produce the desired vehicle acceleration command vector, λ. A steering logic within the control function converts the guidance acceleration command (λ) into attitude and attitude rate commands. An inner-loop Proportional-Integral-Derivative (PID) feedback control law is applied to attitude and attitude rate errors to gimbal the main engine to rotate/tilt the vehicle and thrust vector it to generate the desired net acceleration. Powered descent and landing utilize both TVC and RCS to execute the guidance acceleration profile required for precision landing (to decelerate and orient the vehicle for pointing of ALHAT sensors). During the Approach (ALHAT HD) phase, the FCS maintains the vehicle attitude to within ±1°/axis briefly for imaging of the targeted science site to ensure determination of a safe landing site that results in the desired 20 m landing ellipse. Following acquisition of the HD imagery, the FCS resumes the guidance commanded trajectory along the powered descent profile in Figure 5. Similar to the Morpheus vehicle,[31] the NAVIS FCS also includes a vertical control system for generating delta throttle commands that ensure TVD and touchdown at a final descent rate of -1 m/s within ±0.15 m/s.

V.C. Terrain Relative Navigation Design Analysis

The ALHAT-dedicated RAD750 executes the TRN software, which extracts landmark matches by automatically matching local windows of descent image data to the a-priori orbital reconnaissance map stored onboard. The landmark matches are then fused with the IMU data to estimate the position, velocity, and attitude of the vehicle.[18] Benchmarks on the TRN algorithm performance at JPL for Mars descent scenarios have shown that the code running on a RAD750 takes 20 seconds to match three landmarks between a single descent image and a 1024x1024 pixel reconnaissance map. This benchmark was for an extreme Mars landing case where the initial position uncertainty was twice the altitude of the lander. For the MARE lunar scenario, the position uncertainty will never be larger than 1km, which will result in faster processing times. However, for GN&C subsystem concept development the 20-second processing time is used.

The passive optical TRN algorithms and software have been tested extensively in real-time system field tests and in high fidelity simulations of lunar landing. In February and March 2014, the TRN system was tested on a helicopter flying over planetary analog terrain. The TRN system computed position, velocity and attitude in real-time with no human intervention. The position errors when compared to GPS from 100+ runs were contained within a 30m radius circle when the helicopter flew at 3km altitude.[20] In a follow-on test the same system showed position errors less than 3m at and altitude of 300m. These results show that the position error is typically 1% of the altitude, given the existence of orbital reconnaissance maps with pixel sizes on the order of the camera pixel footprint. This rule of thumb is also consistent with off-line landmark matching of airplane field test imagery[32] and full IMU and image fusing from a sounding rocket data set.[33]

Extensive analysis was also performed in simulation to assess TRN performance with respect to lunar terrain and illumination.[32] Figure 6 shows an example descent image and map generated for a 3° sun elevation angle. The terrains and images were generated using the DEMMaker software developed at the Johns Hopkins University Applied Physics Laboratory (APL).[34] Since MARE will be landing near lunar dawn there can be significant shadowing, so the sensitivity of TRN to sun illumination must be understood. Figure 7 shows horizontal position error and success rate (defined as percent of runs with position error less than 100m) for increasing sun elevation angles for the case where the sun elevation angle is the same for

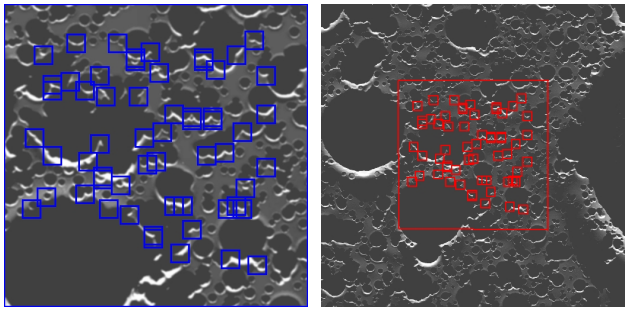

Figure 6. Example descent image (left) and map image (right) with corresponding landmark matches.

the map and the descent image. These results were for terrain that resembles the Aristarchus region (the science target for MARE). TRN is clearly insensitive to sun elevations above 5°, which is less than the 10° sun elevation planned for MARE landing.

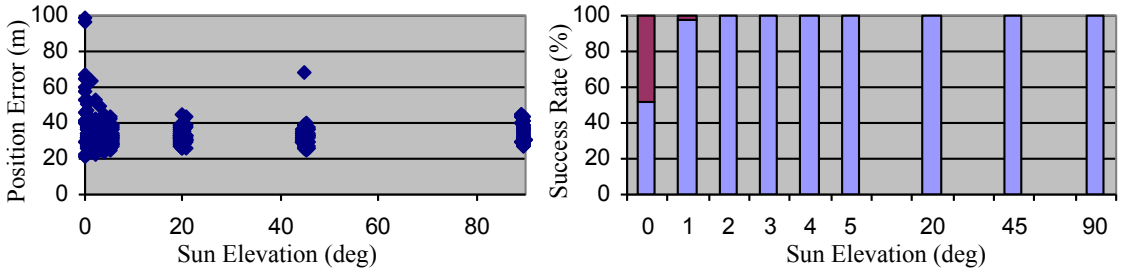

Figure 7. TRN sensitivity to sun elevation angle when map and descent image have the same illumination conditions.

Figure 8 shows the TRN sensitivity when the sun illumination differs between the descent image and map. Sensitivities at 5° and 45° elevation angles bound the 10° condition for MARE. These results show that, in the worst case, the map azimuth can vary by 15° and the map elevation can vary by 1-2° from the descent image. These constraints are fairly tight, but, if necessary, differences in illumination can be mitigated by re-rendering the map to the expected descent image illumination conditions.[32]

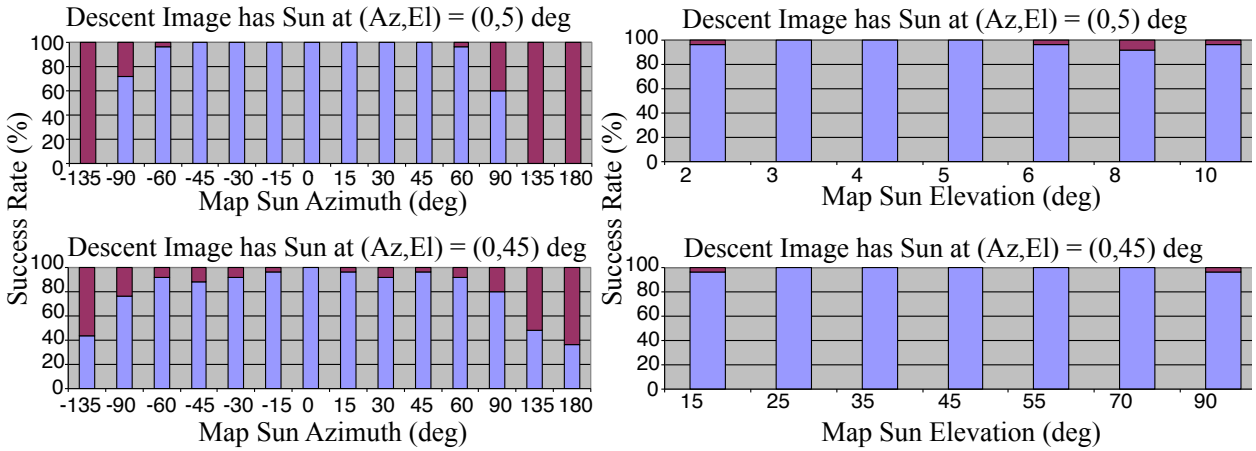

Figure 8. TRN sensitivities when map and descent image have different illumination conditions.

V.D. Landing Risk Assessment and Hazard Detection Design Analysis

A landing risk assessment was performed for the MARE mission to determine the need for an onboard HD system. The assessment was based on Monte Carlos simulations similar to past JPL HD analyses.[30] The assessment incorporates terrain rock abundances, the flash Lidar chosen for the HD system, the geometry and hazard tolerances for the NAVIS spacecraft, and the knowledge uncertainty anticipated from the descent Navigation filter. Figure 9 provides the results of the analysis for safe landing probability with and without onboard HD for a range of rock abundances.

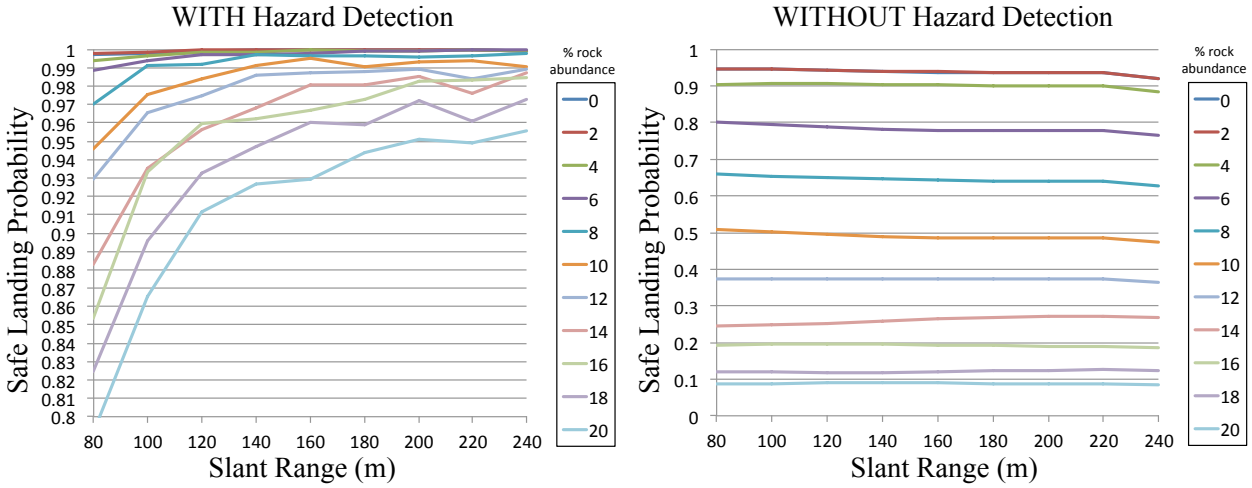

Figure 9. Landing hazard assessment for MARE. Left: the probability of safe landing with onboard hazard detection with respect to slant range and rock abundance. Right: the probability of safe landing without onboard hazard detection (i.e., blind landing).

As shown on the right in Figure 9, even for 0% rock abundance there is still a 5% probability of landing failure without HD due to the modest 10° slope tolerance of the NAVIS spacecraft; this confirms that a HD system is required. As shown in the left plot of Figure 9, when HD is added, the safety of the onboard-determined safe site decreases as the slant range (and image footprint) decreases because there are fewer choices from which to select a safe site. Furthermore, as the rock abundance increases the landing site safety decreases because the terrain is becoming increasingly hazardous. Specifically, this analysis shows that when the slant range is greater than 140m, the HD algorithm selects sites that are 99% safe for rock abundances up to 10%. As shown on the right in Figure 9, this is an improvement from a 50% chance of successful landing to a 99% chance of successful landing. At 20% rock abundance the detection performance degrades to around 93%, at 160m slant range, which is still excellent given that only 10% of the terrain in the range image is actually safe. Overall, the HD system performance makes a dramatic improvement in the probability of safe landing in hazardous terrain.

Design of the HD system design for MARE leveraged previous studies of hazard detection for lunar landing.[35,36] The prior studies indicated that rock hazard detection requires six range samples across the hazard to obtain sufficient measurements to adequately sample the top of the hazard. Furthermore, a hazard needs to be six times the pixel-to-pixel range noise in height before it can be robustly distinguished from the ground plane. When these rules of thumb are applied to the 40cm hazard detection threshold for the NAVIS spacecraft, the Ground Sample Distance (GSD), or spacing between measurements on the ground, needs to be no more than 13cm between samples and the range precision must be better than 6.7cm (1-σ). Note that the GSD spacing makes the reasonable assumption that a hazardous rock's width is twice its height. The ASC GEO3D GoldenEye achieves these requirements. Terrestrial testing with the ASC TigerEye flash Lidar, has shown that each range measurement has a pixel-to-pixel range precision of 6 cm (1-σ); the TigerEye and GoldenEye use the same focal plane array, so the performance will be comparable. From a range of 160 meters, the GoldenEye achieves the 13 cm GSD, which coincides with a 17m $\times$ 17m Lidar image footprint on the terrain surface. For the NAVIS geometry, a 17-meter footprint contains 9 disjoint 5-meter-diameter

regions over which safe sites can be detected. This area is large enough to guarantee a safe landing site within the targeted smooth maria terrain. The 17-meter footprint is also small enough to avoid selection of a safe landing site outside of the 100-meter diameter targeted science ellipse (when considered alongside the precise landing achievable with TRN and NDL sensors, as discussed in Section V.A).

The time available for HD is less than five seconds to allow collection of the flash Lidar image (at the above specified 160 meter range), processing of the HD algorithm on the ALHAT-dedicated RAD750 to determine the safe site, and execution of the divert maneuver in time to transition into TVD from a 50 meter altitude (Figure 5). The single flash Lidar image needed for safe site selection is collected in 0.1 seconds, so most of the HD time is allocated to the safe site selection algorithm. JPL has developed a fast hazard detection algorithm called Simple Safe Site Selection (S4)[30] and has tested it with synthetic flash Lidar images and real TigerEye Images. The algorithm has been benchmarked at 1.25 seconds on a 66MHz flight processor and should be execute in half that time on a 133MHz RAD750 flight processor.

VI. Summary Remarks

The MARE mission proposal was not selected as a 2015 NASA Discovery mission; regardless, the engineering and science teams developed concepts, tools and capabilities that can be leveraged within future proposals and missions. The development of the mission design trajectories and the powered descent operations concept provided specific performance requirements that were leveraged within the NAVIS spacecraft design, making it a flexible architecture that can be adapted for many landing missions. Additionally, with respect to GN&C, the targeted terrain region and the desire for a 20-meter landing ellipse drove navigation analyses and terrain hazard analyses that flowed into GN&C requirements development and supported inclusion of the NASA ALHAT capabilities within the baseline MARE NAVIS design. The subsequent flow-down of performance requirements onto the ALHAT sensors for the MARE mission provided insight into the needs of near-term robotic lander missions that will be leveraged in the continued path-to-spaceflight development work within the NASA ALHAT team. This flow-down also drove the NAVIS avionics analysis of onboard processing architectures and how to host the sophisticated ALHAT algorithms for TRN and HD that enable NAVIS GN&C to safely and precisely deliver science payloads to the targeted surface location.

Acknowledgments

The development of the MARE proposal was a collaborative effort by a large team of engineers, scientists and staff within JSC, SwRI, ASU, JPL, LaRC and many other organizations. We would like to acknowledge the MARE team, the ALHAT team, and the Morpheus team in general for the body of written content and references that we drew from in the development of the MARE proposal and this paper. We would like to specifically acknowledge the support of Eric A. Hurlbert, John C. Melcher, and Robert L. Morehead for their support in conveying the NAVIS Propulsion subsystem content within this paper. Proposal involvement by the Jet Propulsion Laboratory, California Institute of Technology, was performed under contract with NASA (Government sponsorship acknowledged).

References

[1]Epp, C., Robertson, E., and Brady, T., "Autonomous Landing and Hazard Avoidance Technology (ALHAT)," *Proc. IEEE Aerospace Conference (AEROCONF 2008)*, March 2008.

[2]Epp, C. D., Robertson, E. A., and Carson III, J. M., "Developing Autonomous Precision Landing and Hazard Avoidance Technology from Concept through Flight-Tested Prototypes," *Proc. AIAA GN&C Conference*, AIAA 2015-0324, Kissimmee, FL, Jan. 5–8 2015.

[3]Steering Committee for NASA Technology Roadmaps; National Research Council of the National Academies, *NASA Space Technology Roadmaps and Priorities: Restoring NASA's Technological Edge and Paving the Way for a New Era in Space*, The National Academies Press, 2012.

[4]Robbins, S., "New crater calibrations for the lunar crater-age chronology," *Earth and Planetary Science Letters*, Vol. 403, 2014, pp. 188–198.

[5]Committee on the Planetary Science Decadal Survey; Space Studies Board; Division on Engineering and Physical Sciences;

National Research Council of the National Academies, *Vision and Voyages for Planetary Science in the Decade 2013-2022*, The National Academies Press, 2012.

[6]Neukum, G., Ivanov, B., and Hartmann, W., "Cratering records in the inner solar system in relation to the lunar reference system," *Space Science Reviews*, Vol. 96, No. 1, 2001, pp. 55–86.

[7]Hartmann, W. and Neukum, G., "Cratering Chronology and the Evolution of Mars," *Space Science Reviews*, Vol. 96, 2001, pp. 165–194.

[8]Fassett, C. and et al., "The global population of large craters on Mercury and comparison with the Moon," *Geophysical Research Letters*, Vol. 38, No. 10, 2011.

[9]Marchi, S. and et al., "Global resurfacing of Mercury 4.0-4.1 billion years ago by heavy bombardment and volcanism," *Nature*, Vol. 499, No. 7456, 2013, pp. 59–61.

[10]Bougher, S., Hunten, D., and Phillips, R., *Venus II–geology, geophysics, atmosphere, and solar wind environment*, Vol. 1, University of Arizona Press, 1997.

[11]Marchi, S. and et al., "The violent collisional history of asteroid 4 Vesta," *Science*, Vol. 336, No. 6082, 2012, pp. 690–694.

[12]Schenk, P. and et al., "The geologically recent giant impact basins at Vesta's south pole," *Science*, Vol. 336, No. 6082, 2012, pp. 694–697.

[13]Schmedemann, N. and et al., "Crater retention ages from (4) Vesta matching independent Ar-Ar ages of HED meteorites," *EGU General Assembly Conference Abstracts*, 2013.

[14]Michel, P. and Morbidelli, A., "Review of the population of impactors and the impact cratering rate in the inner solar system," *Meteoritics and Planetary Science*, Vol. 42, 2007, pp. 1861–1869.

[15]Johnson, A. and Ivanov, T., "Analysis and Testing of a LIDAR-Based Approach to Terrain Relative Navigation for Precise Lunar Landing," *Proc. AIAA Guidance, Navigation, and Control Conference*, August 2011.

[16]Trawny, N., Carson, J. M., Huertas, A., Luna, M. E., Roback, V. E., Johnson, A. E., Martin, K. E., and Villalpando, C. Y., "Helicopter Flight Testing of a Real-Time Hazard Detection System for Safe Lunar Landing," *Proc. AIAA SPACE 2013 Conference & Exposition*, San Diego, CA, 10–12 Sept. 2013.

[17]Epp, C. D., Robertson, E. A., and Ruthishauser, D. K., "Helicopter Field Testing of NASA's Autonomous Landing and Hazard Avoidance Technology (ALHAT) System fully integrated with the Morpheus Vertical Test Bed Avionics," *Proc. AIAA SPACE 2013 Conference & Exposition*, San Diego, CA, Sept. 2013.

[18]Johnson, A., Bergh, C., Cheng, Y., et al., "Design and Ground Test Results for the Lander Vision System," *36^{th} Annual AAS Guidance and Control Conference*, AAS 13-042, Breckenridge, CO, Feb. 1–6 2013.

[19]Trawny, N., Huertas, A., Luna, M. E., Villalpando, C. Y., Martin, K., Carson, J. M., Johnson, A. E., Restrepo, C., and Roback, V. E., "Flight testing a Real-Time Hazard Detection System for Safe Lunar Landing on the Rocket-Powered Morpheus Vehicle," *Proc. AIAA GN&C Conference*, AIAA 2015-0326, Kissimmee, FL, Jan. 5–8 2015.

[20]Johnson, A. E., Cheng, Y., Montgomery, J., Trawny, N., and Zheng, B. T. J., "Real-Time Terrain Relative Navigation Test Results from a Relevant Environment for Mars Landing," *Proc. AIAA GN&C Conference*, AIAA 2015-0851, Kissimmee, FL, Jan. 5–8 2015.

[21]Carson III, J. M., Robertson, E. A., Trawny, N., and Amzajerdian, F., "Flight Testing ALHAT Precision Landing Technologies Integrated Onboard the Morpheus Rocket Vehicle," *Proc. AIAA Space 2015 Conference & Exposition*, Pasadena, CA, August 2015.

[22]Hurlbert, E. A., Morehead, R. L., McManamen, J. P., Hernandez, H., Melcher, J. C., Collins, J. A., and Guymon, A. W., "System Level Trade Studies, Design, Test, and Operation of the Morpheus Vertical Test Bed for Liquid Oxygen and Methane Technology for Spacecraft Applications," *62nd JANNAF Propulsion Meeting (JPM)*, Nashville, TN, June 2015.

[23]Strahan, A. and Hernandez Jr, H., "Slosh Baffle Design and Test for Spherical Liquid Oxygen and Liquid Methane Propellant Tank for a Lander," *47th AIAA/ASME/SAE/ASEE Joint Propulsion Conference & Exhibit*, AIAA 2011-5633, July 2011.

[24]Hurlbert, E. A., Desai, P., and Guardado, H. J., "Differential Draining of Parallel-Fed Propellant Tanks in Morpheus and Apollo Flight," *62nd JANNAF Propulsion Meeting (JPM)*, Nashville, TN, June 2015.

[25]Melcher, J. C., Morehead, R. L., Atwell, M. J., and Hurlbert, E. A., "Design and Test of a 2,000 lbf Liquid Oxygen / Liquid Methane Thruster with Heat Flux Measurement," *62nd JANNAF Propulsion Meeting (JPM)*, Nashville, TN, June 2015.

[26]McManamen, J. P., Hurlbert, E. A., and Kroeger, D. J., "Development and Flight Operation of a 5 lbf to 20 lbf O2/CH4 Roll Control Engine for Project Morpheus," *62nd JANNAF Propulsion Meeting (JPM)*, Nashville, TN, June 2015.

[27]Amzajerdian, F., Pierrottet, D., Petway, L., Hines, G., and Barnes, B., "Doppler lidar sensor for precision navigation in GPS-deprived environment," *Proc. International Society for Optics and Photonics (SPIE)*, June 2013.

[28]Pierrottet, D. F., Amzajerdian, F., Petway, L. B., Hines, G. D., and Barnes, B., "Field Demonstration of a Precision Navigation Lidar System for Space Vehicles," *Proc. AIAA Guidance, Navigation, and Control Conference*, Boston, MA, August 2013.

[29]Carson, J. M., Bailey, E. S., Trawny, N., Johnson, A. E., Roback, V. E., Amzajerdian, F., and Werner, R. A., "Operations Concept, Hardware Implementation and Ground-Test Verification of a Hazard Detection System for Autonomous and Safe Precision Lunar Landing," *AAS/AIAA Astrodynamics Specialist Conference*, AAS 13-856, Hilton Head, SC, Aug. 11–15 2013.

[30]Johnson, A. and Mandalia, A., "Simple Safe Site Selection: Hazard Avoidance Algorithm Performance at Mars," *37^{th} Annual AAS Guidance and Control Conference*, AAS 14-083, Breckenridge, CO, February 2014.

[31]Jang, J., Yang, L., Fritz, M., Nguyen, L., Johnson, W., and Hart, J., "Design and Analysis of Morpheus Lander Flight Control System," *AAS/AIAA Astrodynamics Specialist Conference SPACE Conference and Exposition*, AIAA 2014-4115, August 2014.

[32]Cheng, Y., Clouse, D., Johnson, A., Owen, W., and Vaughan, A., "Evaluation and Improvement of Passive Optical Terrain Relative Navigation Algorithms for Pin-Point Landing," *AAS Space Flight Mechanics Meeting*, January 2011.

[33]Mourikis, A., Trawny, N., Roumeliotis, S., Johnson, A., Ansar, A., and Matthies, L., "Vision Aided Inertial Navigation for Spacecraft Entry Descent and Landing," *IEEE Transactions on Robotics and Automation*, Vol. 25, No. 2, 2009, pp. 264–280.

[34]Shankar, U., Shyong, W. J., Criss, T. B., and Adams, D., "Lunar Terrain Surface Modeling for the ALHAT Program," *AIAA/IEEE Aerospace Conference*, March 2008.

[35]Johnson, A., Huertas, A., Werner, R., and Montgomery, J., "Analysis of On-Board Hazard Detection and Avoidance for Safe Lunar Landing," *IEEE Aerospace Conference (AEROCONF 2008)*, March 2008.

[36]Johnson, A., Keim, J., and Ivanov, T., "Analysis of Flash Lidar Data Field Test Data for Safe Lunar Landing," *Proc. IEEE Aerospace Conference (AEROCONF 2010)*, March 2010.